Functionalizing graphene oxide framework membranes with sulfonic acid groups for superior aqueous mixture separation

COMMUNICATION

Functionalizing graphene oxide framework membranes with sulfonic acid groups for superior aqueous mixture separation†

Received 00th January 20xx,
Accepted 00th January 20xx

DOI: 10.1039/x0xx00000x

Guang Yang,[ab] Zongli Xie,*[b] Marlene Cran,[a] Derrick Ng,[b] Christopher D. Easton,[b] Mingmei Ding,[c] Hang Xu[c] and Stephen Gray*[a]

Hydrophilic pervaporation (PV) membranes with ultrahigh throughput and outstanding separation ability are highly beneficial for efficient separation of aqueous mixtures. However, it is still challenging to obtain high selectivity without compromising water permeation flux for state-of-the-art PV membranes. Herein, a sulfosuccinic acid (SSA) covalently linked graphene oxide (GO) membrane is developed via a facile vacuum filtration process on a nylon substrate followed by heat treatment. During the membrane fabrication process, ester groups form through the dehydration condensation reaction between -COOH from the SSA and -OH from the GO. The resultant graphene oxide framework (GOF), with well defined two dimensional nanocapillaries functionalised by unreacted -SO_3H, features enhanced hydrophilicity and remarkable swelling resistance, leading to excellent separation performance with ultrahigh water permeation fluxes and precise molecular sieving properties towards both dehydration of alcohol and desalination. This research provides a strategy to dramatically enhance the performance by adding unreacted, additional functional groups into the GOF membranes.

Two-dimensional (2D) graphene oxide (GO) laminar assembly[1] with well-ordered microscopic structure has been appealing as a new type of membrane since the paper-like GO was first realized by vacuum filtration in 2007.[2] Unlike traditional polymer membranes, which usually have randomized pores, cylindrical pores or non-pores,[3-5] the GO laminar membrane is composed of the nanosheets stacked in parallel with each other to produce horizontal 2D nanometer capillaries (2D nanochannels), *i.e.* the void spaces between the adjacent GO monolayers. Molecules transport tortuously through the network of the GO boundary-connected nanocapillaries as the GO monolayer is impermeable. This unique laminar membrane structure endows the GO membrane with its excellent separation properties. Nair *et al.*[6] found that the GO laminar membrane allowed the transport of molecules fitting inside the nanochannel while larger molecules were blocked. The 2D nanochannel shows molecular sieving effects towards solutes of variable sizes. Since GO is hydrophilic owing to the presence of polar oxygen-containing functional groups including epoxide, hydroxy, carboxyl, and carbonyl on the basal planes and edges, it also exhibits outstanding water selectivity for various aqueous mixtures such as saline water and water/solvents. Jin and co-workers investigated the separation of water and dimethyl carbonate (DMC) by pervaporation (PV). Even though the diameter of DMC (0.47-0.63 nm) was smaller than the 2D nanochannel (~0.8 nm), 95.2 wt% water content in the permeate was obtained.[7] The results indicated that the GO membrane exhibited preferential water sorption against DMC. Furthermore, the GO membrane shows almost barrier-free permeation of water due to the low-friction flow through the capillaries. It has been reported that the permeation of water molecules is at least 10^{10} times faster than that of helium.[8] All these exceptional features of the GO laminar membrane make it a promising candidate for aqueous mixture separation.[9]

Nevertheless, a major limitation for the application of the GO laminar membranes is the enlargement of interlayer spacing (d-spacing) as a result of the intercalation of water molecules, *i.e.* the swelling.[10-11] This phenomenon has been widely reported with the d-spacing found to increase from ~0.8 to ~1.3 nm in aqueous environments.[12-15] Considering the thickness of graphite or well-reduced GO monosheet (*ca.* 0.34-0.40 nm),[16-17] the 2D nanochannel is accordingly increased from ~0.46 nm to ~0.90 nm. In that case, the elevation in the 2D nanochannel size will subsequently deteriorate the separation capacity. Since the formation of the GO laminar membrane is mainly based on the interlamellar π-π and hydrogen bonding interactions,[18-19] periodically bridging the GO nanosheets by stronger interactions such as covalent bonding to form an interconnected graphene oxide framework (GOF) membrane is a judicious strategy for restraining the swelling and enhancing the stability.[20-23] Hung and co-workers obtained various diamine crosslinked GOF membranes with d-spacing from 0.93 to 1.09 nm in the wet state whereas that of the control GO membrane increased from 0.85 to 1.31 nm.[14] Sun *et al.* employed thiourea to crosslink GO, resulting in a narrowed 2D nanochannel.[24] The d-spacing augmentation of the thiourea crosslinked GO laminar membrane in water was only 11% as compared with 37% for the pristine GO laminar membrane. For the GOF membranes, however, it is still challenging to obtain high separation efficiency without a sacrifice in flux. One of the key factors that requires attention is the physicochemical property of the crosslinker and it is

[a] *Institute for Sustainable Industries and Liveable Cities, Victoria University, PO Box 14428, Melbourne, VIC 8001, Australia. Email: stephen.gray@vu.edu.au*
[b] *CSIRO Manufacturing, Private bag 10, Clayton South, VIC 3169, Australia. Email: zongli.xie@csiro.au*
[c] *College of Environmental Science, Hohai University, 1 Xikang Road, Nanjing 210098, China.*
Electronic Supplementary Information (ESI) available: See DOI: 10.1039/x0xx00000x
Raw experimental data available: https://data.csiro.au/dap/landingpage?pid=csiro:40679

acknowledged that the size of the crosslinker plays an important role in determining the interlayer spacing.[25] Narrowing the d-spacing of GO laminar membrane enables the separation of water from other small molecules such as methanol but concurrently suppressing the transport of water.[16, 24] Moreover, the chemical reaction between GO and the abovementioned crosslinkers inevitably consumes or transfers the pristine functional groups into other forms, leaving only alkyl chains or aromatic rings bridging the neighboring GO nanosheets. That results in a decrease in the hydrophilicity of the GOF membrane.[26] For PV dehydration of alcohol or desalination, enhancing the hydrophilicity while controlling the swelling of the GOF membranes is favorable to obtain high separation performance. In order to realize that, a molecule with moderate size and additional functional groups in conjunction with the reactive groups may be a suitable candidate as a crosslinker. Sulfosuccinic acid (SSA), with a size ≈ 0.6 nm and two carboxyl groups which could react with hydroxy groups on GO, and one additional sulfonic group attached on the carbon chains,[27] is one such molecule with the potential to interlink the GO nanosheets.

Herein, a novel kind of GOF membrane, *i.e.* GO crosslinked with SSA supported by nylon substrate (GOF-SSA) was designed and fabricated by the vacuum-assisted self-assembly process. The GO nanosheets were bonded with SSA via an esterification reaction whereby the sulfonic groups were kept intact and linked with the GO nanosheets via SSA. The swollen GOF-SSA membrane had a reduced 2D nanochannel size of ≈ 0.59 nm, much smaller than that of control GO membrane (≈ 0.90 nm). In particular, introducing sulfonic groups into the GOF membrane improved hydrophilicity. The as-prepared GOF-SSA membrane with a thickness of ≈ 50 nm was applied for PV separation of different aqueous mixtures, including dehydration of alcohol and desalination. Unprecedentedly high throughput with outstanding separation efficiencies was obtained. The GOF-SSA membrane exhibited superior separation performance to state-of-the-art PV membranes reported so far.

As shown in Fig. 1, the formation of the GOF-SSA membrane is realizd by facile vacuum filtration of an aqueous mixture of GO and SSA through the nylon substrate (Details of the membrane synthesis process, pervaporation test and characterization provided in the ESI†). Upon application of vacuum, the mixture of GO nanosheets and SSA was deposited rapidly onto the nylon surface. As water passed through the filter, the concentration of GO nanosheets in the mixture increased, resulting in a significant decrease in the intermolecular distance and increased interactions. During the subsequent filtration period, the content of water continued decreasing and the GO nanosheets were more likely to be aligned on top of each other with SSA sandwiched in the ever-growing deposit. Sheet-to-sheet interactions squeezed and pushed out the remaining water

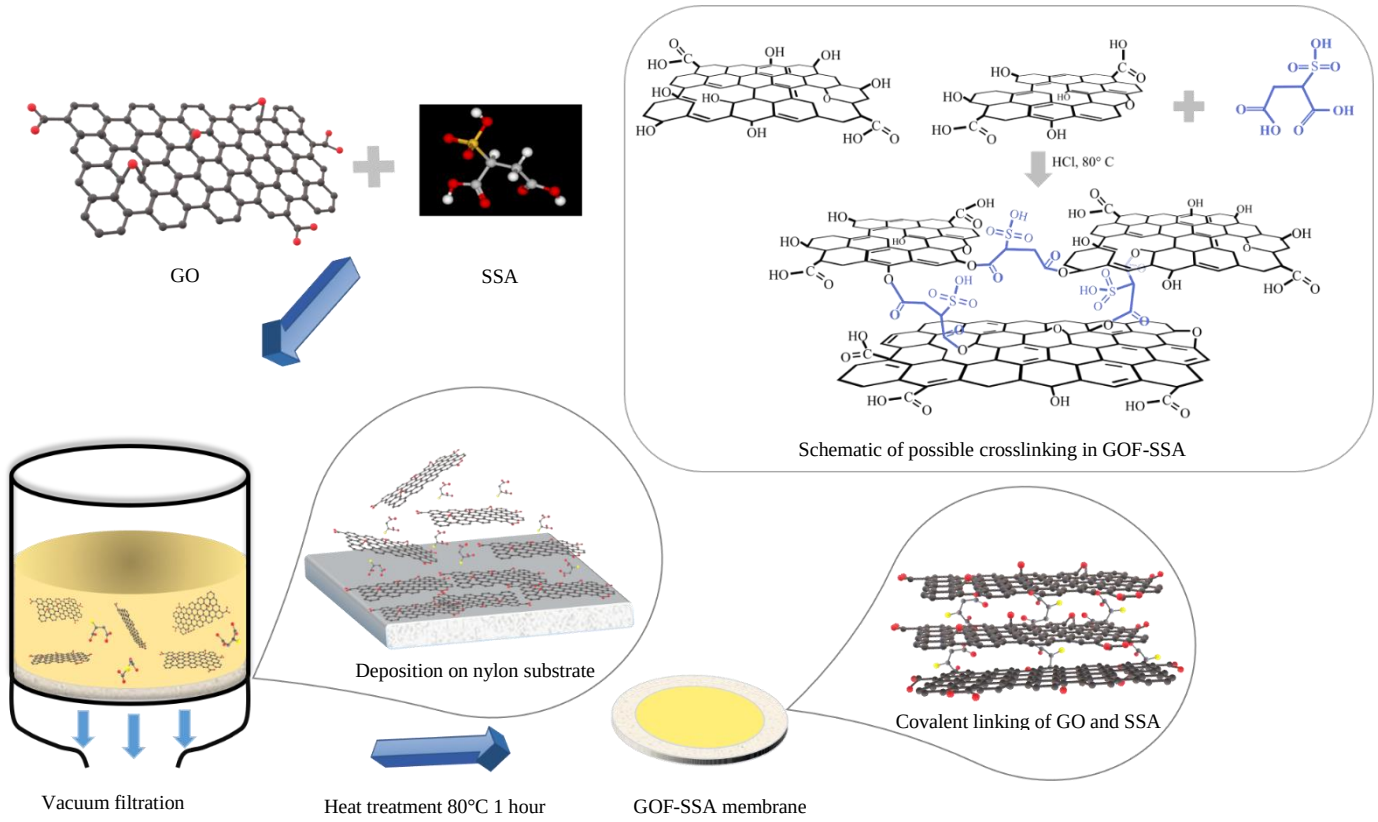

Fig. 1 Formation of GOF-SSA on nylon substrate with possible scheme of crosslinking reaction inserted.

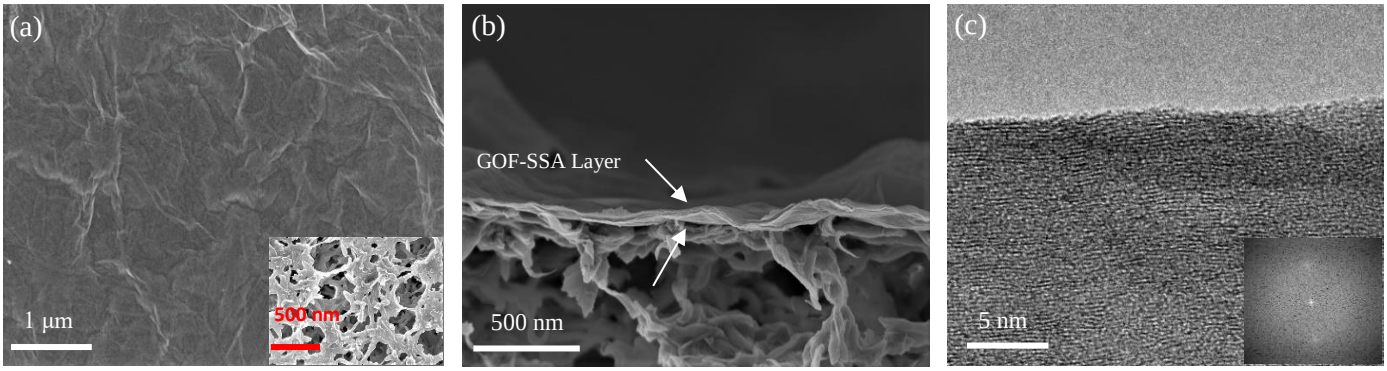

Fig. 2 (a) SEM surface of GOF-SSA with nylon substrate surface SEM inserted, (b) SEM cross-section view and (c) TEM cross-section view of GOF-SSA with FFT image inserted.

molecules, leaving only those that are immobilized as well as SSA until the deposit was relatively dry. Finally, for the catalysis of surface grafting and the crosslinking reaction, a predetermined amount of SSA and then hydrochloric acid (HCl) was added on the surface and filtered through the as-prepared membrane followed by heat treatment at 80°C for 1 hour. After that, the GOF-SSA membrane was immersed in deionized water to remove unreacted SSA. The reaction scheme inserted will be discussed in the characterization part below. The same fabrication method was applied using succinic acid (SA) as the crosslinker to obtain a SA crosslinked GO membrane (GOF-SA) as well as fabrication of a pure GO membrane (control GO) for comparison. Images of the GOF-SSA membrane after immersion in DI water and dried in ambient environment are shown in Fig. S1†.

It is well known that water fluxes are generally inversely proportional to the membrane thickness because the permeation path will be extended with increasing thickness.[28] On that basis, the desired membrane thickness should be as thin as possible to achieve high water flux. The thickness of the GOF layer on the nylon substrate can be tuned from a micrometer scale to a nanometer scale by adjusting the volume of GO solution. The optimized thickness of a GOF-SSA layer with stable and robust performance was ≈ 50 nm considering repeatability and stability. When the thickness was reduced, defects in the GOF layer could be easily observed using scanning electron microscopy (SEM) (Fig. S2†). Adjusting the mass ratios between GO and SSA for the GOF-SSA membrane influences membrane formation and the membrane with the highest rejections of salts and alcohols (GO : SSA = 1:10) is herein characterized. The SEM image of the GOF-SSA surface morphology is shown in Fig. 2a. It can be seen that a rough, dense and homogeneous coverage on the nylon substrate (inserted image) with typical wrinkles resulted. Atomic force microscopy (AFM) measurement of the GOF-SSA membrane surface demonstrated a smoother surface with roughness (Rq ≈ 63.7 nm) compared with the control GO membrane (Rq ≈ 86.2 nm) (Fig. S3†), which may be caused by the presence of SSA in the filtrating mixture with the effect of regulating the stacking manner of the GO nanosheets.[29,30] A cross-sectional view of the GOF-SSA membrane is displayed in Fig. 2b, which reveals that the horizontally stacked nanosheets were compactly assembled onto the nylon substrate. The highly ordered and well-packed 2D lamellar structure of the GOF-SSA layer was further confirmed by the transmission electron microscope (TEM) cross-section view in Fig. 2c. Derived from the fast Fourier transform spectroscopy (FFT) results, the interlayer spacing of the GOF-SSA was ≈ 0.9 nm determined by calculating the repeating units. Energy dispersive spectrum analysis (EDS) was employed here to investigate the elemental

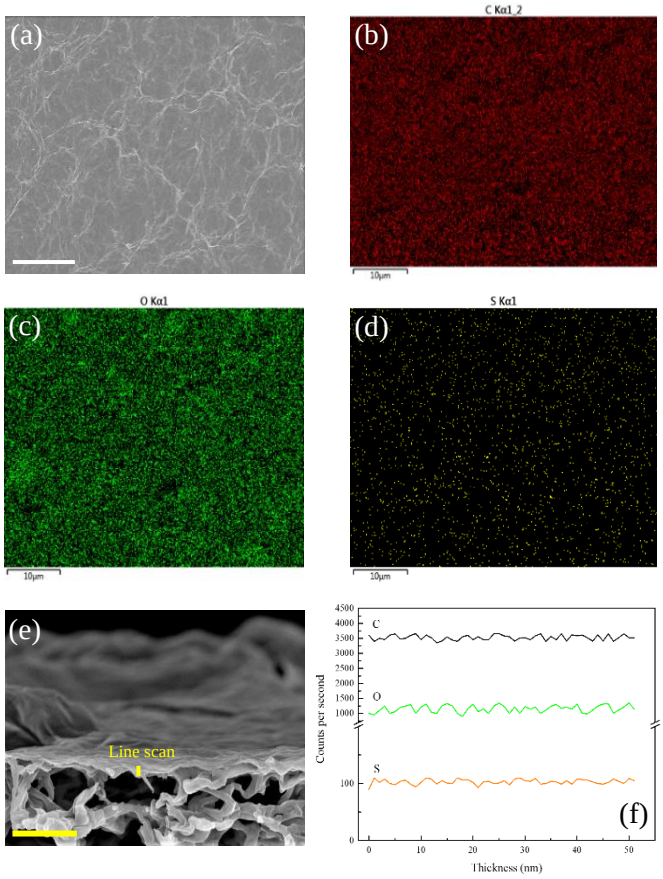

Fig.3 (a-d) EDS elemental mapping of C, O and S on the surface of GOF-SSA fragment. Scale bar 10 μm. (e, f) EDS line scan of C, O and S on the cross-section of GOF-SSA fragment. Scale bar 0.5 μm.

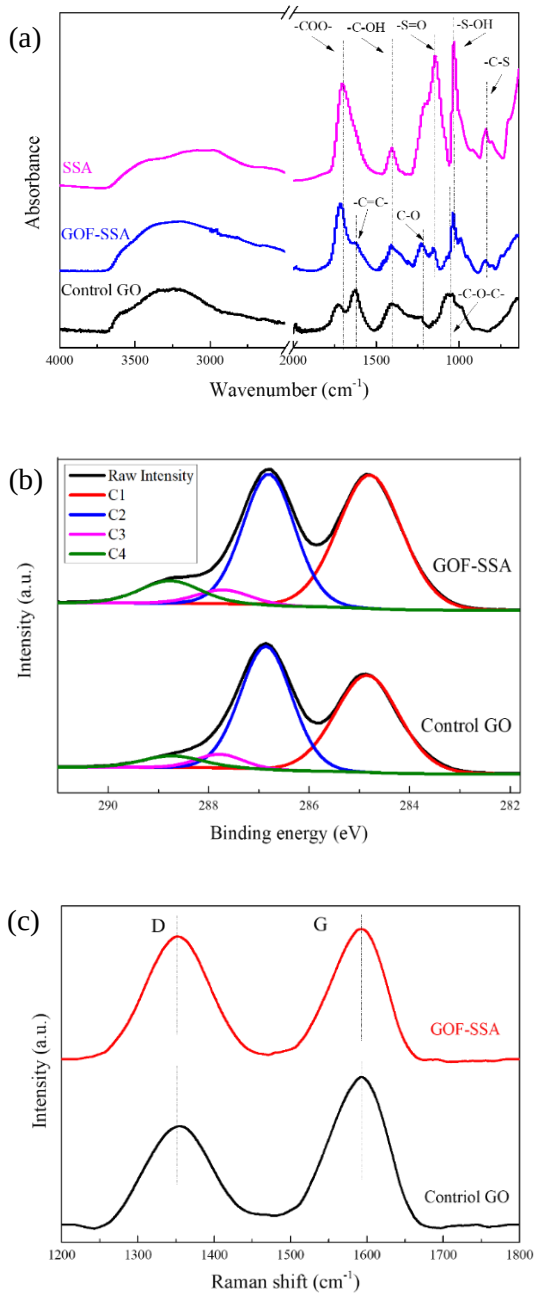

Fig. 4 Chemical properties of GOF-SSA and control GO; (a) FTIR comparison between GOF-SSA, SSA and control GO; (b) XPS spectra fitted with a 4 component system of GOF-SSA and control GO, where the assignments for the components are as follows: C1: C=C/C-C/C-H/C-S; C2: C-O-C/C-OH; C3: C=O and; C4: O-C=O, and (c) Raman results of GOF-SSA and control GO.

distribution (Fig. 3a-d) and it showed that C, O and S were evenly distributed on the surface of GOF-SSA. Correspondingly, EDS line scan profiles of the cross-section were obtained (Fig. 3e-f). Consistent with the surface EDS results, S was also detected with homogeneous longitudinal allocation across the GOF-SSA layer. All the EDS compositions of the GOF-SSA in Fig.3 is listed in Table S1†. Since pure GO contains no S (with the possible exception of impurities), it was not surprising that no S was detected in the control GO and GOF-SA membranes (Fig. S4†).

A comparison between SSA, GOF-SSA and control GO membranes was performed using attenuated total reflectance Fourier transform infrared spectroscopy (ATR-FTIR) measurements to identify the chemical structure as shown in Fig. 4a. The characteristic peaks for GO and SSA are marked (Details discussed in Fig.S5†). For the SSA, the peaks at 725 cm^{-1}, 1048 cm^{-1}, 1184 cm^{-1}, 1375 cm^{-1} and 1725 cm^{-1}, represent C-S stretching vibrations, S-OH stretching vibrations, S=O stretching vibrations, C-OH deformation vibration and carboxylic C=O stretching vibrations, respectively.[31-34] For the GOF-SSA, it is obvious that the intensity of characteristic peaks of ester groups (C=O at 1725 cm^{-1} and C-O at 1330-1000 cm^{-1}) are significantly increased, indicating that these groups are generated during the GOF-SSA membrane fabrication. Meanwhile, the GOF-SSA spectrum exhibits new peaks at 725 and 1184 cm^{-1} that are attributed to the C-S and S=O modes. The intensity of peak at 1045 cm^{-1} remained the same with a sharpened pattern possibly due to the overlapping of S-OH and C-O-C stretching. These results directly demonstrate the presence of functional structures of SSA in GOF-SSA membrane. To verify that statement, FTIR spectra of a vacuum filtered GOF and SSA mixture without catalyst and heat treatment (precursor GOF-SSA) was obtained for comparison (Fig. S5a†). It is notable that there are no characteristic peaks of SSA, but only characteristic bands for GO. This implies that SSA may be physically intercalated in the GO instead of chemical bonding or removed during the immersion in water. For the GOF-SA sample (Fig. S5b†), an obvious increase at 1725 cm^{-1} and 1220 cm^{-1} can be observed, suggesting that GO chemically reacted with SA forming ester groups, in line with previous work.[35]

X-ray photoelectron spectroscopy (XPS) analysis was conducted to further investigate the covalent bonding of GOF-SSA. According to the survey spectra (Fig. S6†), C1s and O1s peaks are observed for all samples, while for the GOF-SSA sample, new peaks associated with S (S2p and S2s) are observed. A more detailed summary of the elemental states and composition is shown in Table S2†. Considering the high O/C ratio for SSA (O : C = 1.75) and the predicted esterification between SSA and GO, it is reasonable to expect that the overall O/C ratio would increase for GOF-SSA. Excluding the possibility of S impurities in GO from the manufacturing process, the S/C atomic ratio (1.1at%) of GOF-SSA was notably increased compared with the control GO and GOF-SA samples and this provides evidence of the presence of S, or groups containing S, in agreement with the ATR-FTIR results. The corresponding high-resolution C1s XPS spectra of the control GO and GOF-SSA samples are depicted in Fig. 4b. C1s spectra were fitted using a total of 4 components, with binding energy positions of approximately 284.8 eV (C1: C=C/C-C/C-H/C-S), 286.8 eV (C2: C-O-C/C-OH), 287.8 (C3: C=O) eV and 288.8 eV (C4: O-C=O). Compared with the control GO sample, the C4/C1 ratio of GOF-SSA was increased by 36.4%, whereas the ratio of

C2/C1 decreased 20.4%. In other words, the relative fraction of C2, which is assigned to C-OH and C-O-C, declined relative to GO while that of C4 (O-C=O) increased. Considering the unchanged intensity of epoxy groups from FTIR results, it is reasonable to conclude that the reactive -OH groups are consumed via the dehydration condensation reactions with -COOH of SSA. For the GOF-SA sample (Fig. S7† and Table S2†), similar observations were obtained.

According to Raman spectroscopy (Fig. 4c), the spectrum of the control GO shows a G band at 1590 cm^{-1} and a D band at 1364 cm^{-1}. The resulting I_D/I_G value of the control GO is 0.89. In contrast, an obvious increase in the intensity of the D band for GOF-SSA was observed and the corresponding I_D/I_G is 1.01. The increased intensity of the D band indicates an elevation in the content of disordered carbon, which may have originated from the chemical linkage of the SSA with GO. The Raman shift of GOF-SA is also displayed for comparison (Fig. S8†), and the value of I_D/I_G is 1.04, which exhibits good agreement in trend with that of GOF-SSA.

Based on the FTIR, XPS and Raman analyses, possible binding approaches between GO and SSA are herein demonstrated whereby there is an esterification reaction between the carboxy groups of SSA and the hydroxy groups of the GO, resulting in the formation of covalent bonds. As SSA contains two carboxy groups at both ends of the molecule, it can act as a bridge to interlink the neighboring GO nanosheets. That results in constructing a crosslinked network of laminated nanocapillaries with sulfonic groups incorporated as shown in Fig.1 (the inserted reaction scheme).

Depending on the fabrication method and environmental humidity, the d-spacing of the GO laminar membrane is normally in the range of 0.6 nm to 1 nm.[7] In the wet state of the GO membrane, the in-plane hydrogen bonds and π-π interactions suffer interference by the incorporation of water molecules, resulting in an enlarged d-spacing. As shown in Fig. 5a, the d-spacing of the control GO and GOF-SSA were analyzed using X-ray diffraction (XRD). For the control GO sample, the intense peak of graphene oxide (001) located at 2θ = 11.5 ° is converted into a d-spacing of 0.79 nm according to the Bragg equation.[36] After immersion in deionized water, it shifted down to 6.94 ° with a corresponding d-spacing of 1.27 nm, showing a 60.8% expansion. In contrast, the XRD pattern of GOF-SSA sample remains relatively stable dwindling from 9.75° for the dry state to 9.15° for the wet state, implying that the d-spacing is increased from 0.90 nm to 0.96 nm. Compared with the control GO, only a 6.7% elevation in the d-spacing for the GOF-SSA is observed. This shows evidence that the crosslinking of GO could effectively restrain the stretching of interlayer spacing by covalently bridging the GO flakes. Accordingly, the 2D nanochannel sizes in the wet state for the control GO and GOF-SSA are 0.90 ± 0.03 nm and 0.59 ± 0.03 nm, respectively. The XRD pattern for GOF-SA is also presented (Fig. S9†) with similar results showing good agreement that the expansion was significantly resisted with d-spacing of 0.89 nm for the dry state and 0.93 nm for the wet state (4.5% increase in d-spacing). Furthermore, if the crosslinking is perpendicular to the GO sheets, the 2D nanochannel size should be just determined by the

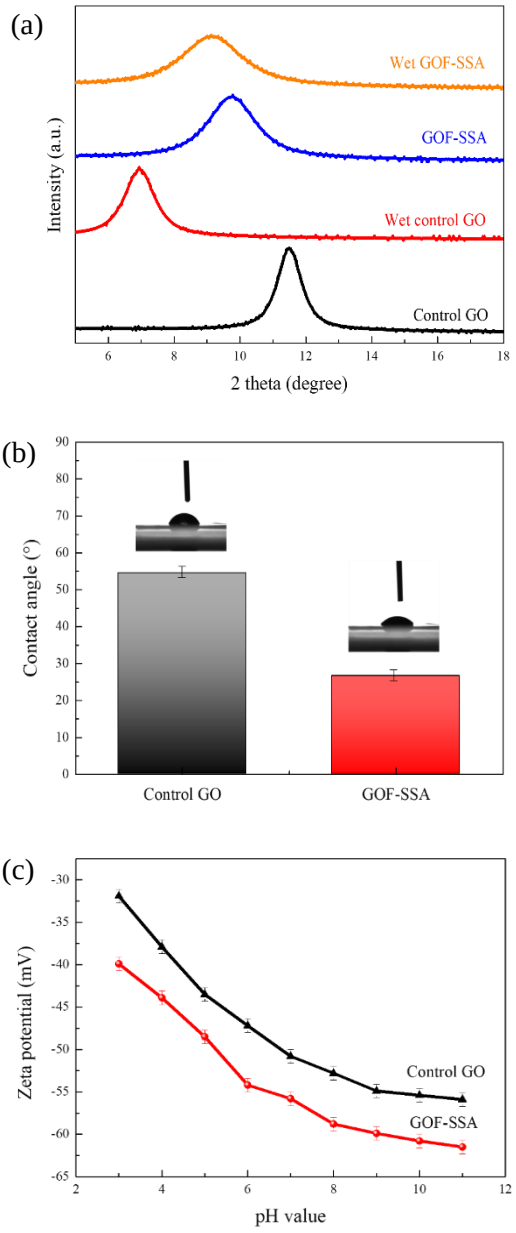

Fig. 5 (a) Comparison between GOF-SSA and control GO before and after incorporation of water, (b) WCA comparison of control GO and GOF-SSA membrane, and (c) zeta-potential of GOF-SSA and control GO samples in the pH value range from 3 to 11.

carbon chain length. Dekany et al. and Nguyen *et al.*[37-38] studied the influence of the crosslinker on the d-spacing both experimentally and theoretically using different aliphatic carbon chain lengths (n=2, 4, 8, 12). They found that a tilted orientation of the crosslinker inside the GO nanochannel is more likely than a perpendicular orientation, suggesting a smaller d-spacing than the theoretical calculation. In the present study, the size of SSA is ~0.60 nm along the carbon chain direction, which is slightly larger than the dry state d-spacing (~0.59 nm) and it is therefore proposed that SSA may be aslant linked with GO nanosheets (Fig. S10†).

The influences of crosslinking exerted on the surface hydrophilic property of the as-prepared GOF membranes was further explored by the water contact angle (WCA) test shown in Fig. 5b. The WCA of the control GO membrane is 54.5°, in good agreement with previous reports,[14, 26] whereas that of the GOF-SSA is 26.6°. When encountering water molecules, the sulfonic groups chemically grafted onto the GO surface would be protonated, which becomes more hydrophilic than the three membered epoxide rings of GO or -OH groups, thus exhibiting greater hydrophilicity compared with the control GO membrane. A more hydrophilic surface will therefore be favorable for water adsorption. Contrary to expectations, the WCA of the GOF-SA membrane is increased slightly to 65.6° (Fig. S11†), which may be due to the transfer of the -OH groups to esters with much smaller hydration numbers, showing reduced hydrophilicity reported by Shikata *et al.*[39]

The surface charge of control GO and GOF-SSA was measured by zeta potential analysis as shown in Fig. 5c. It reveals that both samples are negatively charged with gradually enhanced electronegativity in the range of pH from 3 to 11. For the control GO sample, the values of the zeta potential decreased with increasing pH and reached a minimum value of -54.1 mV at pH 11. The surface negativity of GO is predominantly derived from the deprotonation of the phenolic hydroxyl and carboxylic acid groups on the surface of the GO sheets. In contrast, the GOF-SSA sample is more negative and the zeta potential values of GOF-SSA also decrease with the pH, showing the lowest value of -62.6 mV. This may be attributed to the attachment of the negatively charged -SO_3H groups onto the surface of the GO nanosheets which is in accordance with the FTIR and XPS results. The GOF-SA sample is the least charged membrane (Fig. S12†), which may be due to the formation of less polar ester groups on the surface.

The PV desalination of 3.5 wt% NaCl solution or equivalent molar concentration of other saline solutions was conducted, and the results are shown in Fig. 6a. The salt rejections are 99.92% for KCl, 99.90% for NaCl, 99.98% for Na_2SO_4, 99.98% for $MgCl_2$, and 99.98% for $MgSO_4$. For applications involving real water, it is possible that the swelling of GO may be affected by the presence of salts due to a charge screening effect that compresses the electrostatic double layer, thus dramatically decreasing the d-spacing as the ionic strength increases.[11] Therefore, the corresponding wet state XRD patterns of the GOF-SSA after immersing in the as-mentioned saline solutions were conducted (Fig. S13†). The expansion was further suppressed with the d-spacing ranging from 0.95 nm to 0.93 nm, *i.e.* the corresponding 2D nanochannel size is 0.57 ± 0.02 nm to 0.55 ± 0.02 nm, smaller than that in DI water (0.59 ± 0.02 nm). For GO laminar membrane, the separation mechanism is mainly based on the molecular sieving effect that the 2D nanochannel can repel larger ions or solvents while smaller molecules can pass through. The effective hydrated sizes of ions are 0.66 nm for K^+, 0.66 nm for Cl^-, 0.72 nm for Na^+, 0.76 nm for SO_4^{2-} and 0.86 nm for Mg^{2+} [6, 16, 40] and based on these hydrated radii, the ions will be expected to be rejected. To maintain charge neutrality, cations and anions transport through the membrane stoichiometrically, which results in the permeation of ions being

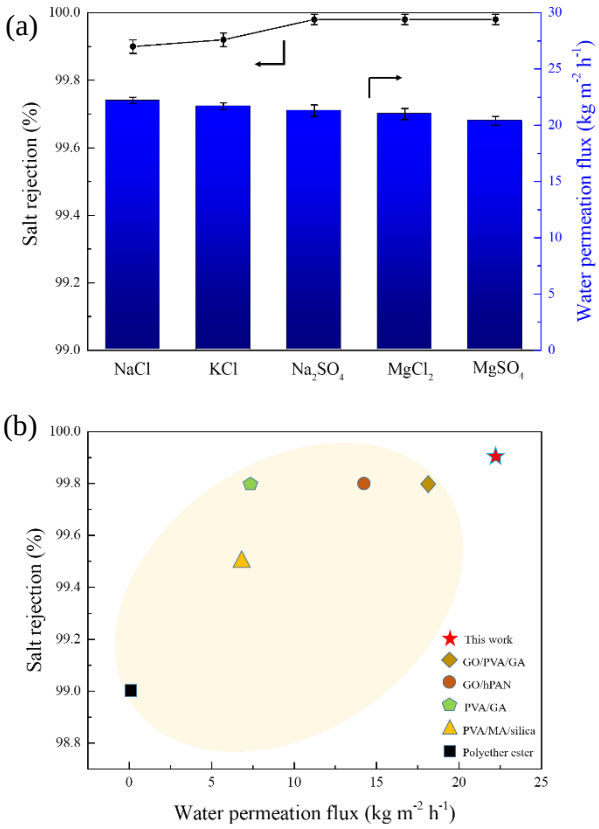

Fig. 6 (a) Desalination of saline solution by GOF-SSA membrane. PV temperature is 30 °C and the pressure on the permeate side of the membrane cell was maintained at 133.3 Pa. Standard deviation was shown as error bar. (b) Comparison of the result in this work with other results by others for desalination using NaCl as feed.

primarily determined by the larger sized ion of the ion-pair. Water molecules, however, will permeate readily through the GOF-SSA membrane owing to their kinetic diameter of 0.29 nm, which is much smaller than the 2D nanochannel size of the wet-state GOF-SSA. In comparison, the control GO membrane shows poor ion rejection and stability with a decline of water flux during the experiment (Fig. S14†). This may be due to the enlarged d-spacing and possible crystal formation of salts on the downstream side. Since salts such as NaCl are non-volatile, it is possible that crystal formation or precipitation would reduce the effective permeation area of the GO membrane, blocking the transport of water. To investigate this, both the upstream and downstream sides of the membranes after the PV test were examined using EDS and salt crystals were found on both the upstream and downstream sides of the GO membrane, whereas no salts were observed for the GOF-SSA membrane (Fig. S15†). This visibly confirms that salt transported readily through the GO membrane and precipitated out on the permeate side. For the GOF-SA membrane, good salt rejection was also achieved (Fig. S16†) with a water permeation flux (for PV of NaCl solution) of 12.13 kg m^{-2} h^{-1}, whereas that of the GOF-SSA membrane was 22.25 kg m^{-2} h^{-1}, showing 83.3% increase. Generally, the PV performance is determined by preferential sorption capacity of

the surface and the diffusivity of permeates through the membrane. Since the GOF-SSA membrane has higher hydrophilicity than GOF-SA and the control GO, more water would be adsorbed during the PV process. On the other hand, the hydrophilic oxygen-containing groups at the edges and surface of the GO nanosheets results in water molecules intercalating into the 2D nanochannel. The presence of sulfonic groups between the GO nanosheets of GOF-SSA, herein, may further facilitate the intercalation of water molecules due to their high hydrophilic and hygroscopic property[41], and thus obtain a high water permeation flux. However, for the GOF-SA membrane, the lower hydrophilicity adversely influenced the water transport by hindering the adsorption of water and subsequently less water permeated through the membrane. Upon increasing the feed temperature, the GOF-SSA membrane achieved an ultrahigh water permeation flux of 80.1 kg m^{-2} h^{-1} at 70°C with a 3.5 wt% NaCl feed solution (Fig. S17a†). The Arrhenius equation was applied to calculate the activation energy (Ea) of water permeation (3.5 wt% NaCl solution as feed) in the PV process with the membranes. Compared with the control GO (23.69 kJ mol^{-1}) and GOF-SA (21.83 kJ mol^{-1}), the GOF-SSA has the highest Ea (26.60 kJ mol^{-1}), indicating that the permeation of water through GOF-SSA is more sensitive to temperature than the control GO and GOF-SA membranes (Fig. S17d†). Finally, the GOF-SSA also shows excellent long-term stability after 50 hours of continuous operation (Fig. S17e†). A performance comparison between GOF-SSA and other membranes reported recently[26, 42-45] has been conducted (Fig. 6b). Both the water permeation flux and salt rejection of GOF-SSA membranes reported herein are the highest of those values obtained under similar operational temperatures (30 °C) and salt concentration (3.5 wt% NaCl solution), providing superior separation performance for the PV desalination.

To further evaluate the performance of GOF-SSA membrane for aqueous separation, the dehydration of alcohol–water binary mixtures (80 wt% of methanol, ethanol, iso-propanol or iso-butanol and 20 wt% water) at 30 °C using GOF-SSA was also investigated and the results are shown in Fig. 7a. The water concentrations in the permeate side were 99.61 wt% for methanol dehydration, 99.83 wt% for ethanol dehydration, 99.94 wt% for iso-propanol dehydration and 99.96 wt% for iso-butanol dehydration. The results are calculated into separation factors (α) of H_2O to C2-C4 alcohol all above 1000. Similarly, the XRD pattern of the alcohol-water mixture all showed reduced d-spacing growth (0.94-0.92 nm) compared with that in the DI water (Fig. S18†). Based on the molecular sieving mechanism, larger-size alcohols such as ethanol, iso-propanol (IPA) and iso-butanol (IBA), with hydrated size of ~0.68, ~0.90 and ~1 nm, respectively,[46-48] will be reasonably excluded. For the dehydration of methanol-water mixture, the size of hydrated methanol (~0.57 nm) is almost equivalent to the 2D channel width of wet-state GOF-SSA (0.56 ± 0.02 nm), which implies that the intercalation of methanol would be possible upon the dehydration of the surrounding water layer. Therefore, the enhanced hydrophilicity of the GOF-SSA membrane, together with the steric hindrance from both the 2D nanochannel and the transporting water molecules are negatively affecting the insertion and diffusion of hydrated methanol, resulting in a much slower permeation than water, in line with previous work.[7] A comparison of the activation energy of permeation for both methanol and water during the PV process using the Arrhenius equation was applied. The results indicated that the Ea (26.60 kJ mol^{-1}) of water was slightly higher than that of methanol (24.31 kJ mol^{-1}), indicating that water transport through the membrane was more responsive to temperature (Fig. S19†). For the GOF-SA membrane, taking the dehydration of methanol for comparison (Fig. S20†), the separation performance was not as good as that of the GOF-SSA membrane, possibly due to the declined hydrophilicity lowering the selectivity towards water molecules. The separation performance of the control GO was incomplete due to the swelling and lack of molecular sieving effect as expected (Fig. S21†). Finally, methanol dehydration of the GOF-SSA membrane was evaluated by comparison of the separation performance with those of other types of membranes (Fig. 7b). The use of polymeric membranes generally results in a trade-off phenomenon where the separation factors decrease as the liquid fluxes increase. However, it can be seen that the performance of the GOF-SSA membrane is beyond the upper

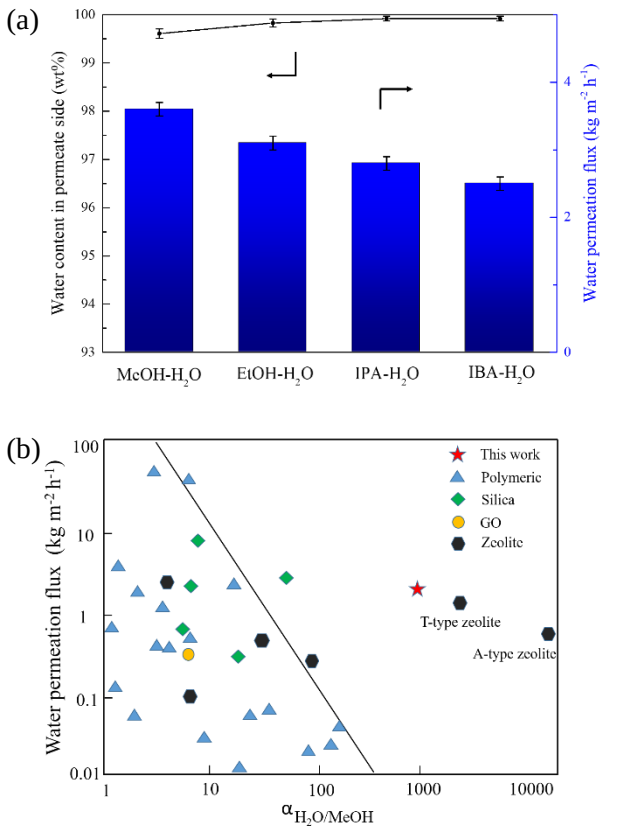

Fig. 7 (a) Dehydration of alcohol–water by GOF-SSA membrane using the same temperature and pressure as that of desalination process. Standard deviation was shown as error bar. (b) Comparison of the H_2O/methanol separation performance of GOF-SSA membrane with literature data (Oblique line: upper bound of polymeric membrane).

bound of polymeric membranes, with higher water permeation flux than those of T-type zeolite and A-type zeolite membranes.[49-51]

In summary, hydrophilic SSA was employed to interlink the GO nanosheets through esterification reaction, leading to the restricted swelling of the GOF-SSA and excellent molecular sieving ability. The hydrophilicity of the GOF-SSA was improved benefitting from the unreacted sulfonic groups. Meanwhile, the new 2D nanochannel of GOF-SSA functionalized by sulfonic acid groups (from SSA) enhanced the separation performance of the GOF membrane. The GOF-SSA membrane exhibited ultrahigh water permeation fluxes with outstanding separation efficiencies towards desalination and solvent dehydration, exceeding the upper bound of state-of-the-art PV membranes. Functionalizing GOF membrane with additional hydrophilic groups demonstrates a rational way to obtain high performance membrane for water purification.

Conflicts of interest

There are no conflicts to declare.

Acknowledgments

The authors would like to acknowledge the financial support from Victoria University and CSIRO Manufacturing. Guang Yang gratefully acknowledges the scholarship from China Scholarship Council (CSC). Special thanks are given to Dr. Julian Ratcliffe (CSIRO) for TEM characterizations and Madeline Van Dongen (Swinburne University of Technology) for assisting with Raman analysis in this work.

Notes and references

1 P. Sun, K. Wang and H. Zhu, *Adv. Mater.* 2016, **28**, 2287-2310.
2 D. A. Dikin, S. Stankovich, E. J. Zimney, R. D. Piner, G. H. Dommett, G. Evmenenko, S. T. Nguyen and R. S. Ruoff, *Nature* 2007, **448**, 457-460.
3 X. Cheng, F. Pan, M. Wang, W. Li, Y. Song, G. Liu, H. Yang, B. Gao, H. Wu and Z. Jiang, *J. Membr. Sci.* 2017, **541**, 329-346.
4 P. D. Chapman, T. Oliveira, A. G. Livingston and K. Li, *J. Membr. Sci.* 2008, **318**, 5-37.
5 M. A. Shannon, P. W. Bohn, M. Elimelech, J. G. Georgiadis, B. J. Marinas and A. M. Mayes, *Nature* 2008, **452**, 301-310.
6 R. K. Joshi, P. Carbone, F. C. Wang, V. G. Kravets, Y. Su, I. V. Grigorieva, H. A. Wu, A. K. Geim and R. R. Nair, *Science* 2014, **343**, 752-754.
7 K. Huang, G. Liu, Y. Lou, Z. Dong, J. Shen and W. Jin, *Angew. Chem. Int. Ed. Engl.* 2014, **53**, 6929-6932.
8 R. R. Nair, H. A. Wu, P. N. Jayaram, I. V. Grigorieva and A. K. Geim, *Science* 2012, **335**, 442-444.
9 B. Mi, *Science* 2014, **343**, 740-741.
10 J. Abraham, K. S. Vasu, C. D. Williams, K. Gopinadhan, Y. Su, C. T. Cherian, J. Dix, E. Prestat, S. J. Haigh, I. V. Grigorieva, P. Carbone, A. K. Geim and R. R. Nair, *Nat Nanotechnol* 2017, **12**, 546-550.
11 S. Zheng, Q. Tu, J. J. Urban, S. Li and B. Mi, *ACS Nano* 2017, **11**, 6440-6450.
12 B. Feng, K. Xu and A. Huang, *RSC Advances* 2017, **7**, 2211-2217.
13 S. Xia, M. Ni, T. Zhu, Y. Zhao and N. Li, *Desalination* 2015, **371**, 78-87.
14 W. S. Hung, C.-H. Tsou, M. De Guzman, Q.-F. An, Y.-L. Liu, Y.-M. Zhang, C.-C. Hu, K.-R. Lee and J.-Y. Lai, *Chem. Mater.* 2014, **26**, 2983-2990.
15 J. Y. Chong, B. Wang and K. Li, *Chem. Commun.* 2018, **54**, 2554-2557.
16 B. Qi, X. He, G. Zeng, Y. Pan, G. Li, G. Liu, Y. Zhang, W. Chen and Y. Sun, *Nat Commun* 2017, **8**, 825.
17 D. H. Seo, S. Pineda, Y. C. Woo, M. Xie, A. T. Murdock, E. Y. M. Ang, Y. Jiao, M. J. Park, S. I. Lim, M. Lawn, F. F. Borghi, Z. J. Han, S. Gray, G. Millar, A. Du, H. K. Shon, T. Y. Ng and K. K. Ostrikov, *Nat Commun* 2018, **9**, 683.
18 S. Dervin, D. D. Dionysiou and S. C. Pillai, *Nanoscale* 2016, **8**, 15115-15131.
19 U. Raviv, S. Perkin, P. Laurat and J. Klein, *Langmuir* 2004, **20**, 5322-5332.
20 L. Dong, W. Fan, X. Tong, H. Zhang, M. Chen and Y. Zhao, *J. Mater. Chem. A* 2018, **6**, 6785-6791.
21 T. Gao, H. Wu, L. Tao, L. Qu and C. Li, *J. Mater. Chem. A* 2018, **6**, 19563-19569.
22 L. Cseri, J. Baugh, A. Alabi, A. AlHajaj, L. Zou, R. A. W. Dryfe, P. M. Budd and G. Szekely, *J. Mater. Chem. A* 2018, **6**, 24728-24739.
23 F. Fei, L. Cseri, G. Szekely and C. F. Blanford, *ACS Appl Mater Interfaces* 2018, **10**, 16140-16147.
24 J. Yang, D. Gong, G. Li, G. Zeng, Q. Wang, Y. Zhang, G. Liu, P. Wu, E. Vovk, Z. Peng, X. Zhou, Y. Yang, Z. Liu and Y. Sun, *Adv. Mater.* 2018, **30**, 1705775-1705783.
25 J. Zhu, J. Hou, A. Uliana, Y. Zhang, M. Tian and B. Van der Bruggen, *J. Mater. Chem. A* 2018, **6**, 3773-3792.
26 C. Cheng, L. Shen, X. Yu, Y. Yang, X. Li and X. Wang, *J. Mater. Chem. A* 2017, **5**, 3558-3568.
*27 S. Sasikala, K. H. Gopi and S. D. Bhat, Microporous Mesoporous Mater. 2016, **236**, 38-47.*
28 Y. P. Tang, D. R. Paul and T. S. Chung, *J. Membr. Sci.* 2014, **458**, 199-208.
29 X. Tang, Y. Qu, S.-L. Deng, Y.-Z. Tan, Q. Zhang and Q. Liu, *J. Mater. Chem. A* 2018, **6**, 22590-22598.
30 Y. Kang, Y. Xia, H. Wang and X. Zhang, *Adv. Funct. Mater.* 2019, 1902014.
31 Q. Wang, Y. Lu and N. Li, *Desalination* 2016, **390**, 33-46.
32 H. Y. Hwang, H. C. Koh, J. W. Rhimc and S. Y. Nam, *Desalination* 2008, **233**, 173-182.
33 H. Su, P. Zhu, L. Zhang, F. Zhou, X. liang, T. Li, Q. Wang, R. Sun and C. Wongcd, *Sustainable Energy Fuels* 2017, **1**, 1601-1610.
34 Z. Zhang, L. Zou, C. Aubry, M. Jouiad and Z. Hao, *J. Membr. Sci.* 2016, **515**, 204-211.
35 Z. Jia and Y. Wang, *J. Mater. Chem. A* 2015, **3**, 4405-4412.
36 L. B. Zhang, J. Q. Wang, H. G. Wang, Y. Xu, Z. F. Wang, Z. P. Li, Y. J. Mi and S. R. Yang, *Composites: Part A* 2012, **43**, 1537–1545.
37 A. B. Bourlinos, D. Gournis, D. Petridis, T. s. Szabo, A. Szeri and I. De´ka´ny, *Langmuir* 2003, **19**, 6050-6055.

38 S. Stankovich, D. A. Dikin, O. C. Compton, G. H. B. Dommett, R. S. Ruoff and S. T. Nguyen, *Chem. Mater.* 2010, **22**, 4153-4157.
39 T. Shikata and M. Okuzono, *J. Phys. Chem. B* 2013, **117**, 7718-7723.
40 B. Tansel, J. Sager, T. Rector, J. Garland, R. F. Strayer, L. Levine, M. Roberts, M. Hummerick and J. Bauer, *Sep. Purif. Technol.* 2006, **51** 40–47.
41 T. Mitome, Y. Iwai, Y. Uchida, Y. Egashira, M. Matsuura, K. Maekawa and N. Nishiyamaa, *J. Mater. Chem. A* 2014, **2**, 10104–10108.
42 B. Liang, W. Zhan, G. Qi, S. Lin, Q. Nan, Y. Liu, B. Cao and K. Pan, *J. Mater. Chem. A* 2015, **3**, 5140-5147.
43 B. Liang, K. Pan, L. Li, E. P. Giannelis and B. Cao, *Desalination* 2014, **347**, 199-206.
44 Z. Xie, M. Hoang, T. Duong, D. Ng, B. Dao and S. Gray, *J. Membr. Sci.* 2011, **383**, 96-103.
45 E. Quiñones Bolaños, H. Zhou, R. Soundararajan and L. Otten, *J. Membr. Sci.* 2005, **252**, 19-28.
46 B. V. d. Bruggen, J. Schaep, D. Wilms and C. Vandecasteele, *J. Membr. Sci.* 1999, **156**, 29-41.
47 T. Borjigin, F. Sun, J. Zhang, K. Cai, H. Ren and G. Zhu, *Chem Commun (Camb)* 2012, **48**, 7613-7615.
48 C. H. Tsou, Q. F. An, S. C. Lo, M. De Guzman, W.-S. Hung, C.-C. Hu, K.-R. Lee and J.-Y. Lai, *J. Membr. Sci.* 2015, **477**, 93-100.
49 M. Villegas, E. F. Castro Vidaurre and J. C. Gottifredi, *Chem. Eng. Res. Des.* 2015, **94**, 254-265.
50 Y. Tang, N. Widjojo, G. M. Shi, T.-S. Chung, M. Weber and C. Maletzko, *J. Membr. Sci.* 2012, **415-416**, 686-695.
51 P. Shao and R. Y. M. Huang, *J. Membr. Sci.* 2007, **287**, 162-179.